Experimental Investigation of a Direct-Drive Hall Thruster and Solar Array System at Power Levels up to 10 kW

John Steven Snyder,* John R.Brophy,† Richard R. Hofer,‡ Dan M. Goebel, § and Ira Katz**
Jet Propulsion Laboratory, California Institute of Technology, Pasadena, CA, 91109

As NASA considers future exploration missions, high-power solar-electric propulsion (SEP) plays a prominent role in achieving many mission goals. Studies of high-power SEP systems (i.e. tens to hundreds of kilowatts) suggest that significant mass savings may be realized by implementing a direct-drive power system, so NASA recently established the National Direct-Drive Testbed to examine technical issues identified by previous investigations. The testbed includes a 12-kW solar array and power control station designed to power single and multiple Hall thrusters over a wide range of voltages and currents. In this paper, single Hall thruster operation directly from solar array output at discharge voltages of 200 to 450 V and discharge powers of 1 to 10 kW is reported. Hall thruster control and operation is shown to be simple and no different than for operation on conventional power supplies. Thruster and power system electrical oscillations were investigated over a large range of operating conditions and with different filter capacitances. Thruster oscillations were the same as for conventional power supplies, did not adversely affect solar array operation, and were independent of filter capacitance from 8 to 80 μF. Solar array current and voltage oscillations were very small compared to their mean values and showed a modest dependence on capacitor size. No instabilities or anomalous behavior were observed in the thruster or power system at any operating condition investigated, including near and at the array peak power point. Thruster startup using the anode propellant flow as the power 'switch' was shown to be simple and reliable with system transients mitigated by the proper selection of filter capacitance size. Shutdown via cutoff of propellant flow was also demonstrated. A simple electrical circuit model was developed and is shown to have good agreement with the experimental data.

Nomenclature

f_{cm}	=	current degradation factor for panel mismatches in array
f_{vm}	=	voltage degradation factor for panel mismatches in array
G_{sun}	=	solar irradiance, W/m^2
$G_{sun,\ base}$	=	baseline solar irradiance for panel performance data, W/m^2
I_{mpo}	=	panel current at the maximum power point at standard conditions, A
I_{mp}	=	panel current at the maximum power point, after applying degradation and environmental factors, A
I_{sco}	=	panel short-circuit current at standard conditions, A
I_{sc}	=	panel short-circuit current after applying degradation and environmental factors, A
N_s	=	number of solar panels in series for each string
N_p	=	number of parallel strings of solar panels
T_{base}	=	baseline temperature for panel performance data, °C
T_{cell}	=	cell operating temperature, °C
V_{oco}	=	panel open-circuit voltage at standard conditions, V

* Senior Engineer, Electric Propulsion Group, Senior Member AIAA.
† Principal Engineer, Propulsion, Thermal, & Materials Engineering Section, Associate Fellow AIAA.
‡ Senior Engineer, Electric Propulsion Group, Associate Fellow AIAA.
§ Senior Research Scientist, Propulsion, Thermal, & Materials Engineering Section, AIAA Fellow.
** Group Supervisor, Electric Propulsion Group, Senior Member AIAA.

V_{oc}	=	panel open-circuit voltage after applying degradation and environmental factors, V
V_{mpo}	=	panel voltage at the maximum power point, at standard conditions, V
V_{mp}	=	panel voltage at the maximum power point, after applying degradation and environmental factors, V
ΔV_{diode}	=	voltage drop across array blocking diodes, V
ΔV_{wiring}	=	voltage drop in solar array wiring, V
β_{Isc}	=	temperature coefficient for panel short-circuit current, 1/°C
β_{Imp}	=	temperature coefficient for panel max-power current, 1/°C
β_{Vmp}	=	temperature coefficient for panel max-power voltage, 1/°C
β_{Voc}	=	temperature coefficient for panel open-circuit voltage, 1/°C
,array	=	solar array parameter for summed series and parallel arrangement of panels

I. Introduction

The idea for direct drive has been around since at least 1970.[1] The key motivation for the development of direct drive then and now is the desire to significantly reduce the mass of high-power, solar electric propulsion vehicles by eliminating most of the heavy, expensive power conditioning electronics between the solar array and the electric thrusters. In the mid 1970's a key motivation for direct drive technology development was the demanding Comet Halley rendezvous mission for the once-in-a-lifetime return of the comet in 1986. This mission was enabled by solar electric propulsion, but required performance well beyond the state-of-the-art.[2] The state-of-the-art in electric propulsion in the United States in the 1970's was represented by NASA's 30-cm-diameter, mercury-fueled, gridded ion thruster. As with any gridded ion thruster most of the power is processed by the "Beam Supply" that provides the high voltage to accelerate the ionized propellant. By 1976 direct-drive testing was already underway as indicated by Atkins[3] where he refers to the "*already demonstrated operation of some engine components, such as Beam and Discharge, directly from high voltage solar array to reduce power processing requirements*."

In 1977, Gooder[4] describes direct-drive tests that "*were performed in which integrally regulated solar arrays (IRSA's) were used to directly power the beam and accelerator loads of a 30-centimeter-diameter, electron-bombardment, mercury ion thruster*." The motivation for this work, as described by Gooder[3] was that, "*For large electrical loads such as ion thruster and high-power radio frequency amplifiers, the necessary power processors are heavy, complex, and expensive to design and build and are a substantial burden on the spacecraft thermal control system*." The solar array used by Gooder was capable of providing up to 1,200 V at 1.0 A. The array was located indoors and illuminated with a bank of tungsten-iodide lamps. In these tests the NASA 30-cm mercury ion thruster was successfully operated at beam currents of up to 1.0 A at a beam voltage of 1,100 V. Even with no added capacitive filtering between the solar array and the thruster Gooder reported that there were no major differences in the wave-forms for the beam and accelerator currents and voltages compared to those obtained with conventional power supplies. Significantly, the direct-drive configuration easily handled the grid-to-grid arcs typical of gridded thruster operation. Conventional power-processing systems contain circuitry that detects and clears such arcs in a process referred to as a "high-voltage recycle." In the direct-drive mode with solar array segments providing both the beam and accelerator functions, the arrays were simply allowed to "collapse" during an arc which typically cleared the arc naturally and allowed the voltages to recover. Indeed, Gooder notes that, "*A solar array is inherently tolerant of load arcs.*" The very small capacitance of the solar array prevents damage to the grids during arcing events. Based on this work Gooder concluded that, "*the basic characteristics of mercury ion thruster and solar arrays are extremely compatible. Using appropriately designed solar arrays to directly power major thruster loads will produce stable, highly efficient power-processing systems for ion thrusters*."

NASA also investigated other aspects of direct drive for the Comet Halley mission including low-thrust trajectory analysis,[5] investigation of high-voltage (≥ 1 kV) solar array interactions with the plasma environment,[6,7] and systems studies.[8] While ultimately the Comet Halley Rendezvous mission was not implemented, NASA recognized the benefits of direct drive for high-power electric propulsion systems. In his 1978 overview of NASA's electric propulsion technology development program Hudson[9] mentions mission studies with solar array powers ranging from 1 kW to 100 kW and says, "*In the future it may be shown to be feasible to operate thrusters directly from high voltage solar arrays (direct drive), thereby eliminating a significant fraction of the power processing and thermal control system mass requirements*."

After the promising start in the 1970s, there was little work done on direct drive in the 1980s. A major contributing factor for this was the expectation that solar arrays with output voltages of a kilovolt or more, as required by gridded ion thrusters, wouldn't be available any time soon.

In the early 1990s the excellent performance of Hall thrusters developed by the Soviet Union was confirmed.[10] This made high-performance electric thrusters that required DC input voltages of around 300 V available in the West for the first time and immediately revived the interest in direct drive. In this case it would be Hall thrusters, instead of gridded ion thrusters, that would be powered directly by solar arrays with output voltages of a few hundred volts instead of a more than a thousand volts. Both mission and system design[11] and direct-drive testing[12] were resumed. The work described by Hamley[12] represented the resumption of direct-drive testing after a 20-year hiatus. This testing used a 4.5-kW, T-160 model Hall thruster developed by the Keldysh Research Center in Russia and a 1-kW terrestrial, linear concentrator solar array with a concentration ratio of 21-to-1. The array could be configured to provide a maximum voltage of 300 V. It was located outdoors and mounted to a full two-axis sun-tracking mechanism. These tests successfully demonstrated startup and steady-state operation of the T-160 Hall thruster at up to 1 kW at 200 V and 780 W at 300 V, and as with any research activity, raised new questions. While this work was a significant step in the verification of the feasibility of direct-drive, no further direct-drive tests were performed to resolve the new questions that it raised.

In 2001 NASA started a 3-year program to develop a Direct Drive Hall Effect Thruster (D2HET) system with the objective of significantly reducing power processing complexity, weight and cost.[13] This program included understanding the behavior of high-voltage solar arrays in the plasma environment produced by the Hall-thruster based propulsion subsystem,[13-17] and direct-drive systems engineering.[18,19] The systems engineering work, which included Hall thruster testing with a solar array simulator, identified a number of issues that would need to be resolved before direct drive could be implemented. NASA's renewed interest in direct drive stimulated new mission studies,[20] additional systems engineering studies,[21] and investigations of solar array designs for high-voltage operation.[22] No direct-drive testing with an actual solar array was performed under this development activity.

The first direct-drive tests to use triple junction solar cells are described by Brandhorst, et al,[23] in which a 1.3 kW, T-100 Hall thruster from the Keldysh Research Center was operated directly from a triple junction, linear concentrator solar array. The 8-to-1 stretched-lens concentrator solar array used in these tests was mounted outdoors and could produce up to 1.2 kW at 500 V under clear sky conditions. These tests successfully operated the T-100 thruster direct drive at up to 600 W and 550 V.

In 2010 NASA's Human Exploration Framework Team (HEFT) identified that the use of high-power (of order 300-kW) solar electric propulsion (SEP) could cut in half the number of heavy lift launch vehicles required for a human mission to a "hard-to-reach" NEA.[24,25] The very high power level of this vehicle concept made it a natural candidate for direct drive, but serious technical questions made it difficult to baseline the use of direct drive. In 2011 NASA made the decision to implement a National Direct-Drive Testbed to address the technical issues identified in previous direct-drive investigations. This list of technical issues identified in previous studies is given in Table 1. The National Direct-Drive Testbed was designed to perform direct-drive tests at power levels an order of magnitude greater than previous tests and to resolve the issues listed in Table 1. On the strength of this planned test program the Human spaceflight Architecture Team (HAT) changed the baseline concept for the 300-kW SEP vehicle to direct-drive. This paper describes the design of the National Direct-Drive Testbed and the progress made to date in addressing the technical issues in Table 1.

Table 1. List of Identified Direct-Drive Technical Issues.

1	What does the EMI filter need to look like for a direct-drive system?
2	What are the impacts of thruster oscillations on the solar array operation?
3	What are the impacts of thruster oscillations on EMI?
4	What are the impacts of thruster oscillations on the thruster operating point?
5	Do the thruster current oscillations move the array up and down the I-V curve?
6	How do the solar array current/voltage oscillations feed back into and affect the thruster operation?
7	How much filtering is required to mitigate the effect of solar array current/voltage oscillations on the thruster operation?
8	What are the effects of intermittent high current spikes on the system operation?
9	Are there differences in the thruster's volt-amp characteristics when operating direct-drive?
10	Is a shunt regulator required for a direct-drive system?
11	Can a direct-drive system be designed without a shunt regulator?
12	How close to the peak power point can/should the thruster be operated?
13	How do you do this with multiple thrusters?
14	How do you maintain thruster operation on the open-circuit side of the solar array?

15	What do you do if the solar array voltage collapse puts you into a low voltage, high current mode of thruster operation?
16	How do you recover if the solar array voltage collapses during thruster operation?
17	How do you start and stop a thruster in a direct-drive system?
18	How do you switch the solar array voltage to the thruster anode?
19	How do you minimize/prevent current overshoot when starting the thruster?
20	What magnet and flow rate settings are required?
21	How do you transition to steady-state operation?
22	How do you start and operate multiple Hall thrusters in a direct-drive system?
23	How do you enforce cathode current sharing for multiple Hall thrusters in a direct-drive system?
24	Previous tests did not operate the thrusters anywhere close to the thruster's nominal input power design point. For the GRC test the thruster was operated at only 22% of the nominal input power point. For the Auburn test the thruster was operated at 46% of the nominal design power level. What happens when you operate at the nominal power point?
25	Previous direct drive tests only went up to 1 kW. Are new issues encountered when scaling up to 10 kW?
26	How should the spacecraft bus power be provided? (300-V spacecraft bus; down-convert to the spacecraft bus voltage; tapped solar array; separate solar array section for the spacecraft).
27	What additional fault protection is required, i.e., for solar array arcing and/or unacceptable leakage current?

II. Test Setup and Methods

A. Solar Array

The National Direct-Drive Testbed consists of a set of fifty-six commercially-available terrestrial solar panels and a power control station designed specifically to provide flexibility in solar array electrical configuration. Each 1.60 m ×1.06 m panel includes ninety-six 15%-efficient mono-crystalline silicon solar cells and provides 255W of power under Standard Test Conditions.[26] Solar irradiance, cell temperature, and solar spectrum affect the actual output in field use. The panels were installed on available roof space of the Electric Propulsion Laboratory at JPL, as shown in Fig. 1, where a number of engineering and facility constraints drove the final panel layout. The array as installed can produce a maximum of about 12 kW for direct-drive operation under ideal conditions, although for reasonable test durations under typical environmental conditions the maximum useable power is about 10 to 11 kW.

Fig. 1. The National Direct-Drive Testbed Solar Array.

Electrical power is routed through approximately 60 m of cable from the panels to the power control station, which is located immediately adjacent to vacuum chamber used for thruster testing. Eight strings of five panels each are connected in series on the roof then routed to the control station with the remaining sixteen panels routed individually. At the entrance to the control station each of the eight strings and sixteen panels can be individually switched into or removed from active power production. From there a set of thirty-one relays are used to combine the panels in different series and parallel configurations to produce the desired solar array performance curve for direct drive testing.

Under the environmental conditions present during the testing described herein, each panel produced an open-circuit voltage slightly higher than 50 V (depending on cell temperature) and each string of panels produced a short-circuit current of up to roughly 5 A (at solar noon, depending on net solar irradiance). Actual performance varied based on the time of day and environmental conditions. Hence, a string of seven panels could be expected to produce an open-circuit voltage near 350 V and four strings of panels could be expected to produce up to about 20 A. Although many array configurations are possible with the power control station, the testing described herein

was performed with configurations of four to eight strings of four to nine panels each, i.e. open-circuit voltages of approximately 200 V to 450 V and maximum short-circuit currents of approximately 20 to 40 A.

B. Hall Thruster

The H6 is a 6 kW nominal laboratory Hall thruster that was developed as a testbed for studies of thruster physics and developments in diagnostics and thruster technology.[27] The thruster was a joint development between JPL, the University of Michigan, and the Air Force Research Laboratory and continues to be studied at those institutes. The throttling range of the thruster is approximately 0.6-12 kW discharge power, 1000-3000 s specific impulse, and 50-500 mN thrust. Over 70% total efficiency is achieved at discharge voltage of 800 V. At the nominal 300 V, 6-kW condition, thrust, total specific impulse, and total efficiency are 406 mN, 1970 s, and 65%, respectively. A centrally-mounted lanthanum hexaboride cathode was used for this work.

For direct-drive testing, it was expected that the thruster would be operated at a large number of different current-voltage pair operating points because of the constraint of operation on the solar array current-voltage curve. Hence, general rules for magnet currents as a function of discharge power were established and followed during the testing instead of pre-determining optimum magnet currents for every conceivable operating condition. In many cases during testing magnet currents were adjusted as necessary when it was clear that discharge current oscillations exceeded normal levels, but magnet currents were never optimized based on the discharge current or discharge current oscillations at every operating condition.

C. Electrical Schematics

The electrical setup for the Direct-Drive testing is little different than for a test with conventional laboratory supplies. As shown in Fig. 2 the thruster is connected directly to the power source with an intervening filter capacitor. Both solar and conventional power supplies were used to drive the thruster during testing and the configuration was easily switched between the two. The output of the different combinations of solar panels coming from the array power control station is represented in the figure by a single circuit element. The figure does not show the several safety disconnect switches associated with the solar system, nor the cathode clamping circuit used to keep the negative side of the circuit from wandering too far from ground. Also not shown are the conventional cathode heater, cathode keeper, and magnet power supplies that were isolated from the discharge power circuit.

A large 80 μF electrolytic capacitor that is typically used for Hall thruster testing in this facility served as the baseline filter capacitor. For many tests this capacitor was replaced with a capacitor bank comprised of combinations of identical 8.1 μF tantalum capacitors stacked in parallel and in series to produce different net filter capacitance values. A bleed resistor was added to the system for safety.

An SCR thyristor located downstream of the filter capacitor was used to start the thruster for many experiments. It was driven by an external isolated gate circuit and would apply power source voltage to the thruster very rapidly, in less than a microsecond. It was removed from the circuit after early testing demonstrated more benign startup methods.

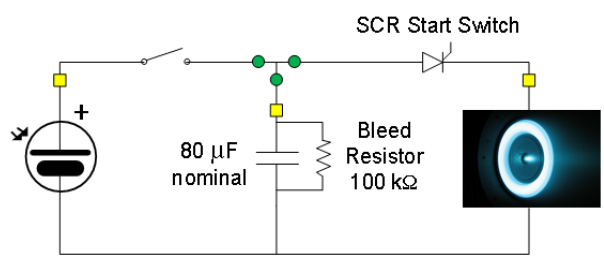

Fig. 2. Direct-Drive Electrical Schematic. The green circles represent locations for current probing; yellow squares represent locations for voltage probing.

Measurement of current and voltage oscillations and startup transients in the system were regularly performed and the locations of those measurements are indicated in the figure. All current measurements were performed at a junction box near the filter capacitor. Array bus voltage measurements were performed on the power control station bus bar where all solar panel strings were collected together, capacitor voltage measurements directly on the capacitor (or capacitor bank), and thruster voltage measurements from a pair of sense lines that exited the vacuum chamber.

D. Test Facility and Instrumentation

All testing was performed in the Al Owens vacuum test facility at JPL. The vacuum chamber is 3 m in diameter and 8.6 m long, with nine cyropumps installed and operational for this testing. With the vacuum chamber configuration used for this test the effective pumping speed was approximately 170,000 L/s on xenon. To minimize facility backsputter rates the interior of the vacuum facility is lined with graphite panels. Electrical power and xenon flow were both provided with standard laboratory systems.

The power system, flow system, and facility telemetry were controlled and monitored with a Labview-based data acquisition and control system. The data system recorded thruster currents, voltages, and flow rates as well as facility and solar array data at a user-specified rate, typically several times a minute. The software used to record data was also used to control thruster power supplies and flow rates.

Global hemispherical solar irradiance was measured in real-time with a dedicated instrument located about 200 m south of the solar array installation. Data were logged using a separate data system, also several times a minute. This instrument was not calibrated prior to testing and was used for indication in combination with a photovoltaic performance model.

A pair of multichannel digitizing oscilloscopes was used to capture electrical system oscillation data and startup transient data. Acquisition of all oscillation data reported here was performed with standard settings of 100,000 points and a sample interval of 1 µs. Voltage oscillations were measured with standard 10× voltage probes; startup transients were measured with a pair of 500× high-voltage differential probes. Current oscillations were measured with a combination of Pearson coils and clamp-on current probes; only the probes were used for startup transients. A direct comparison of data from the coils and probes showed that they were interchangeable for oscillation measurement over the frequency range used here.

Current and voltage oscillation data are presented in this paper as root-mean-square (RMS) values. Oscillation data were acquired with the oscilloscope in AC coupling mode to remove the DC component of the signal, hence the data have a mean value of zero. The RMS oscillation was then calculated using the standard method:

$$RMS\ value\ of\ Y = \sqrt{\left(\frac{1}{M}\sum Y_i^2\right)}$$

where M number of data points are gathered.

E. Solar Array Performance Model

Prediction and understanding of solar array performance curves (current-voltage and power-voltage) were critically important to the design of the Direct-Drive Testbed and for the test operation and data analysis. For these efforts a photovoltaic performance model that was developed for small near-Earth solar electric propulsion missions[28] was adapted for terrestrial use. Baseline panel performance data provided by the solar panel manufacturer[26] were adjusted for solar irradiance and cell temperature using standard cell modeling techniques applied to this design,[29] resulting in the expressions given in Eqs. 1-4:

$$I_{sc} = I_{sco}\frac{G_{sun}}{G_{sun,base}} f_{cm}\{1 + \beta_{I_{sc}}(T_{cell} - T_{base})\} \tag{1}$$

$$I_{mp} = I_{mpo}\frac{G_{sun}}{G_{sun,base}} f_{cm}\left\{1 + \beta_{I_{mp}}(T_{cell} - T_{base})\right\} \tag{2}$$

$$V_{oc} = V_{oco} f_{vm}\left\{1 + \beta_{V_{oc}}\ \ (T_{cell} - T_{base})\right\} \tag{3}$$

$$V_{mp} = V_{mpo} f_{vm}\left\{1 + \beta_{V_{mp}}(T_{cell} - T_{base})\right\} \tag{4}$$

where I_{sc} is the short-circuit current of the panel, V_{oc} is the open-circuit voltage, and I_{mp} and V_{mp} are the current and voltage at the maximum power point, respectively. The baseline panel electrical performance data (I_{sco}, I_{mpo}, V_{oco}, V_{mpo}), baseline environments for those data ($G_{sun,base}$, T_{base}), and the temperature coefficients (β_{Isc}, β_{Imp}, β_{Voc}, β_{Vmp}) were taken from the panel datasheet (in some cases the temperature coefficients were inferred from accompanying data). The current and voltage matching factors (f_{cm}, f_{vm}) account for performance losses due to panel/cell mismatches and fabrication differences (e.g. a string of series-connected panels will provide a current determined by the current of the worst-performing panel). The major driver for the panel current output is the solar irradiance (G_{sun}); temperature effects on current are very small. On the other hand, the cell temperature (T_{cell}) is the only environmental variable affecting the panel voltage output in this model.

For direct-drive operation, the desired solar array current and voltage outputs were built from different combinations of panels connected in series (N_s) and strung in parallel (N_p) as shown in Eqs. 5-8. Each parallel string contained a blocking diode with a forward voltage drop of 0.9 V. Calculation of the I-V curve itself was simplified by assuming a constant voltage drop of 5 V in the power wiring. In this study the formulation of Rauschenbach[29] was used to calculate the I-V curve from the array performance parameters ($I_{sc,array}$, $I_{mp,array}$, $V_{oc,array}$, $V_{mp,array}$).

$$I_{sc,array} = I_{sc} N_p \tag{5}$$

$$I_{mp,array} = I_{mp} N_p \tag{6}$$

$$V_{oc,array} = V_{oc} N_s \tag{7}$$

$$V_{mp,array} = V_{mp} N_s + \Delta V_{diode} + \Delta V_{wiring} \tag{8}$$

For predictive purposes, a separate model for solar irradiance was developed from standard astronomical relationships.[30,31] This model combined with a simple atmospheric loss model[32] was used to predict the solar irradiance for any time of day and day of year at the testbed location. During actual testing solar irradiance data were gathered in real time and entered directly into the photovoltaic model to calculate the I-V curve. The photovoltaic model uses only the solar irradiance and cell temperature as inputs. A thermocouple installed on the backside of one of the panels was used to measure the panel temperature during testing.

In practice the panel mismatch losses and wiring voltage drops were not known for each test configuration, and no effort was made here to do a complete characterization. For this work it was assumed that there were no voltage mismatch losses (i.e. $f_{vm} = 1$). Current mismatch losses could not be ignored; initial single-panel short-circuit current testing after installation showed differences in output current of up to 15% between the greatest and least current output (note that these are not space-rated solar cells, hand-chosen for optimal performance). The current mismatch loss was allowed to vary between 0.86 and 0.91 depending on array configuration as different sets of panels were placed into service. Although the measured panel temperature was not equivalent to the cell temperature it was typically within a few to several degrees centigrade, depending on environmental conditions, as evidenced by routine comparison of the measured and calculated open-circuit voltage. Model calculations presented in this paper use cell temperatures that were chosen to produce the measured open-circuit voltage. The photovoltaic model performance calculations are used here to relate thruster operation and data to the position on the actual array performance curves as traced out by thruster operation. Finally, the model was validated with resistive loads prior to thruster operation.

III. Experimental Results

A. Engine Control and Throttling

Typical operation and control of the Direct-Drive system is shown in Fig. 3 for a test lasting approximately 90 minutes. The solar panels were configured in a 6×6 array that produced an open-circuit voltage of 305 V and a short-circuit current of 29 A just prior to the test. Since the test was performed after solar noon, solar irradiance steadily decreased, with the test ending at a value about 85% of the pre-test value. Anode

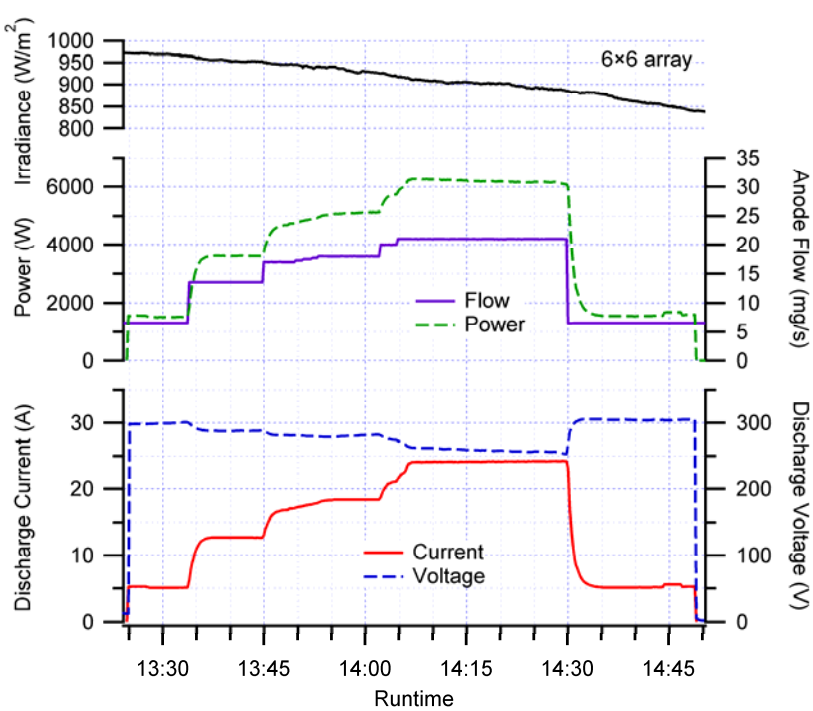

Fig. 3. Direct-Drive Operation and Control up to 6 kW.

flow and magnet currents were initiated prior to engine ignition with an SCR hard-start of the solar array voltage, whereupon the thruster immediately went into operation at 5.3 A and 293 V. The thruster operating point was controlled over the next 45 minutes by stepwise increments in the anode flow rate; the cathode flow rate was changed accordingly to maintain the proper flow fraction, and the magnet currents were adjusted to match those proper for the discharge power. .

After reaching the nominal maximum power of the H6 at 6 kW, the gas flows and magnet currents were held constant for about 25 minutes to operate the thruster discharge in constant-current mode. Finally the thruster power was rapidly decreased by a large stepwise decrease in the anode flow rate. Discharge power quickly fell from 6 kW to 1.5 kW and was held there for the remainder of the test. During this entire test the thruster was easily controlled through the anode flow rate and operation was stable. No anomalous thruster or power system behavior was observed as the thruster was started, slowly ramped to 6 kW operation, rapidly throttled down, then shutdown.

Note that during constant-current operation near 6 kW the thruster discharge voltage steadily decreased by about 10 V. Shown in Fig. 4 and Fig. 5 are thruster data for the 33 minutes enveloping the 6 kW operation, along with calculations from the solar array performance model for the beginning and ending of the 6 kW operation. As the solar irradiance decreases at constant cell temperature this changes the array I-V curve as shown in Fig. 4, reducing the array short-circuit current while holding the open-circuit voltage constant. With a constant-current load this I-V curve change has the effect of reducing array voltage as shown by the 6 kW data in the figure. Note also that this motion of the sun across the sky in a terrestrial application simulates the outbound portion of a planetary spacecraft trajectory, mimicking what a Direct-Drive system would see in application.

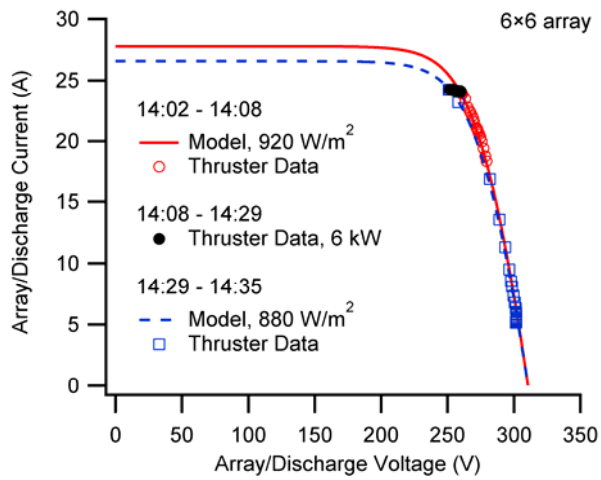

Fig. 4. Current-Voltage Curve for Selected Data of Fig. 3.

The data of Fig. 5Fig. 4 show that during this test the thruster was throttled up the power-voltage (P-V) curve (red circles and model) to 6 kW operation, approaching but not reaching the array peak power point. As the sun moved across the sky the available power from the array was reduced until at the end of the 6 kW period the thruster was operating almost exactly at the array peak power point. During the rapid intentional throttling down the P-V curve (blue squares and model) the thruster power went from 100% to 25% of the array peak power point in six minutes with no thruster stability issues observed. The downward throttling time was limited by the length of tubing between the mass flow controller and the thruster; faster transitions were not possible with this experimental setup.

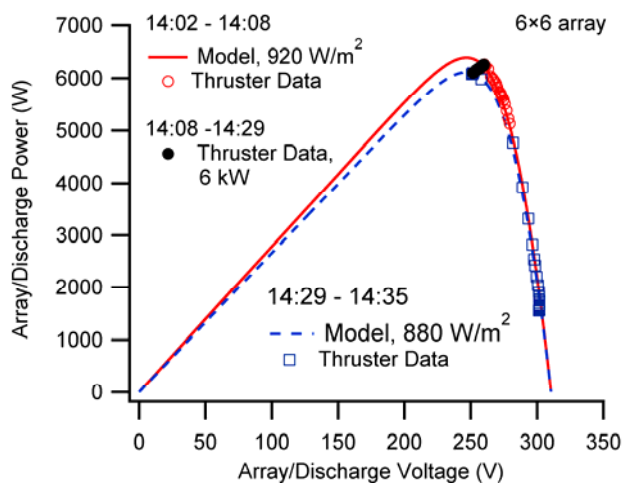

Fig. 5. Power-Voltage Curve for Selected Data of Fig. 3.

Thruster operation was also successfully performed at voltages less than the peak power voltage by increasing the anode flow rate to drive the thruster through and across the peak power point. Shown in Fig. 6 are the runtime data for an afternoon test with a 7×4 array configuration, where the array performance curves for the first 30 minutes of testing are shown in Fig. 7. The thruster was started via anode gas flow initiation (startup methods will be discussed in detail in a later section) and quickly ramped to about 93% of the beginning-of-test peak power. 5000 A combination of small anode flow increases and decreasing solar irradiance brought the operating point across the array peak power point at 297 V to a voltage of 262 V. The system operated stably throughout this process. At this point the thruster jumped into a different operating mode at a much lower voltage and power as seen in the data of Fig. 6. Thruster operation was stable at this lower power point. The physical reason for this mode change has not been explored yet, but it should

be noted that similar mode changes are observed when running up against the current limit in a conventional laboratory power supply, so this effect is not one that is unique to direct-drive power systems. Limited movement along the P-V curve in the low-voltage mode was accomplished via gas flow changes.

Transition back to the higher-voltage operating mode was easily accomplished by reducing the anode flow rate as seen in Fig. 6. In this particular test the flow rate had to be reduced more than was necessary to operate in the higher power mode in order to induce the mode change. Once there the thruster continued to operate nominally in the higher-voltage mode. After a period of constant-current operation in which other diagnostic tests were performed, the thruster was repeatedly driven into and recovered from the low-voltage mode with no issues. At no point during testing of the Direct-Drive system did the array completely collapse and extinguish the thruster. Low-voltage operating modes always existed and higher-voltage operation could always be recovered easily. The relative voltage at which the transition occurred was seen to depend on operating conditions. In Fig. 8 that transition occurred at a point 20 V less than the peak power voltage. At a higher discharge voltage but similar discharge current operating condition, that transition occurred at a point 100 V less than the peak power point (these data are shown in Fig. 14).

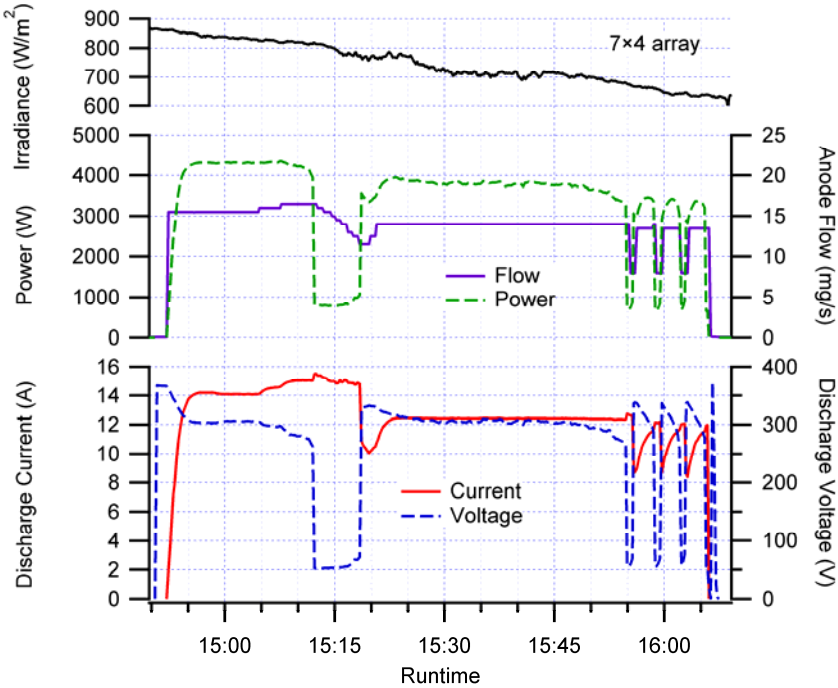

Fig. 6. Direct-Drive Operation and Control Through the Peak Power Point and with Operating Mode Changes.

Although the transition between these operating modes is of interest from a device physics point of view, mission applications for low-voltage, low-power thruster operation are limited. Operation at the peak power point and higher voltages will fulfill most applications of interest. Knowledge of the voltage at which the transition occurs, however, would be of use for spacecraft operators, so this transition warrants further study.

In summary, Hall thruster operation with a direct-drive power system is easily controllable over a wide range of operating conditions via the anode flow rate, just as for operation on conventional laboratory supplies. Thruster operating conditions match the photovoltaic performance model calculations very well.

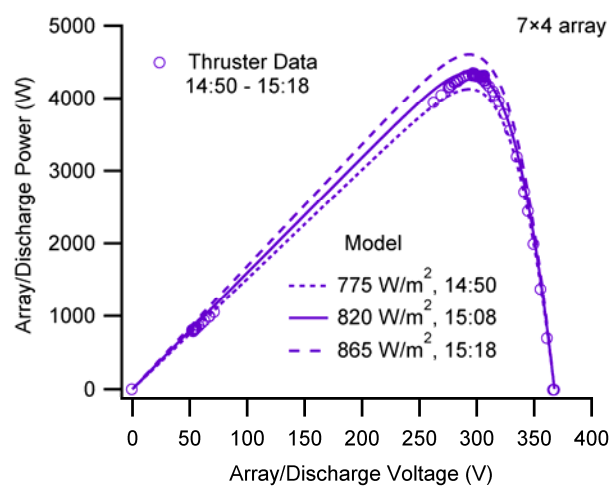

Fig. 7. Power-Voltage Curve for Selected Data of Fig. 6.

B. System Electrical Oscillations

A major portion of this work was to investigate the system electrical stability for a variety of array voltages and power levels across the array P-V curve, specifically to look for instabilities or large oscillations. At many different array configurations the thruster was driven from startup conditions across the peak power point, often to a low-voltage mode of operation, while current and voltage oscillations were recorded with the oscilloscopes. This was done with a variety of different filter capacitances, summarized in Table 2.

A comprehensive set of oscillation data gathered across a wide range of operating conditions is shown in Fig. 8. In this set of tests, a 7×4 array was used for P-V curve sweeps using an 80 µF filter capacitance. In the figure, the discharge voltage at which the oscillation data points were acquired is correlated to the I-V and P-V curves at the bottom of the figure. The first thing to note is that the oscillation magnitudes are all very small compared to the mean currents and voltages. Thruster RMS current oscillations are at most 800 mA, less than 5% of the mean value, and voltage oscillations are at most 1.8 V, less than 0.7% of the mean value. The AC current fluctuations in the filter capacitor are about the same as those in the thruster, and the voltage oscillations about the same as in the array. The array bus oscillations are remarkably small, less than 40 mA and 600 mV, both less than 0.3% of their mean values.

Table 2. Summary of Test Conditions for Oscillation Measurements.

Array Configuration	Filter Capacitance (µF)					
	80	57	32	24	16	8
4×4	✓					
5×4	✓					
6×6		✓	✓	✓	✓	
7×4	✓				✓	✓
7×8	✓					
8×3	✓					
8×4	✓					
8×5	✓				✓	
9×4	✓					

As thruster operation moved from 1 kW to the peak power of 4.5 kW in Fig. 8 the thruster current and voltage oscillations increased slightly, then decreased to a local minimum near the peak power point. A similar but much smaller trend is seen in the array oscillations. Beyond the peak power point, as the array voltage decreased and current increased at constant magnet currents, thruster current oscillations display a noticeably increasing trend yet remain low compared to the mean discharge current. When the engine transitioned into the low-voltage mode of operation the current and voltage oscillations remained quite low. This transition was closely watched for any type of anomalous behavior, but nothing of note was observed. Recall that the magnet current was not optimized to minimize oscillations at all data points, so it is possible that the oscillation trends seen here would be different for optimized thruster operating conditions.

The oscillation data as presented in Fig. 8 are useful yet do not tell the whole story on system oscillations, particularly the changes in frequency content. The frequency dependence of the oscillations was investigated by examining the power spectral density of each individual oscilloscope capture. The power spectral density is a useful tool because the RMS oscillations in any frequency range may be extracted by integrating over the frequency domain and taking the square root of the result. Data for five of the different thruster current oscillation captures from Fig. 8 are shown in Fig. 10. Ignoring the low-voltage mode for the moment, the oscillations show only minor differences except near the breathing mode where the peak frequency varies between 10 to 20 kHz and the RMS oscillations in that frequency range vary from 0.25 to 0.47 A. These breathing-mode differences account for the nearly all of the variations in the RMS oscillations seen in Fig. 8. The low-voltage mode has a breathing-mode peak of similar magnitude but markedly lower frequency, and much lower oscillations at frequencies of 10 to 100 kHz than the other traces. Note further that there are no indications in these data of a unique frequency structure that might indicate an instability. Not shown here, the behavior in capacitor current oscillations is very similar to the thruster current oscillations.

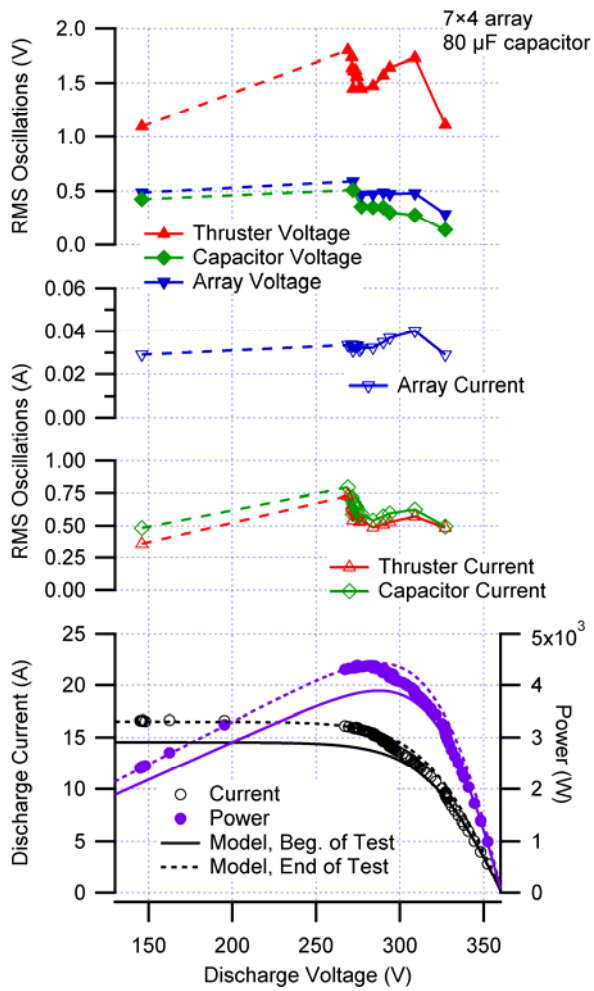

Fig. 8. Direct-Drive System Electrical Oscillations Measured Across the Current-Voltage Curve.

The differences between the curves shown in Fig. 10 are not due to operation with the direct-drive power system, but only to differences in the thruster operating mode. Current oscillation data were also acquired at identical operating conditions using a conventional laboratory supply. When compared to the direct-drive data, as in Fig. 10, the two were found to be nearly identical.

Frequency-dependent oscillations in the array current showed a greater and more interesting dependence on operating condition. As seen in Fig. 11 there is a significant difference in the oscillations at frequencies less than 20 kHz with the highest oscillations occurring at the highest array voltages and vice-versa. Between 20 and 100 kHz there are smaller differences with a reverse order (ignoring the low-voltage mode). Note the logarithmic format of the plot disguises the fact that these competing effects, when integrated over all frequencies, do not show large variations in the RMS oscillations as shown in Fig. 8. Above 100 kHz all data are essentially the same, showing a peak near 200 kHz whose source has not yet been investigated. The low-voltage mode shows markedly different frequency content less than 100 kHz, but 98% of the RMS oscillation magnitude in this condition is at frequencies greater than 100 kHz.

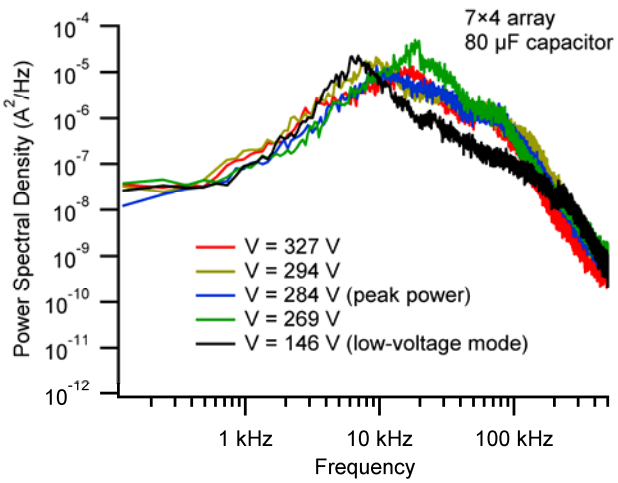

Fig. 9. Thruster Current Frequency Content.

Frequency content of the system voltage oscillations was also examined. None of the sets of traces showed the appreciable systematic differences that the array current oscillations did at lower frequencies, although small, broad differences between traces was observed. Data at all discharge voltages were similar.

The test described in Fig. 8 was next repeated using filter capacitances of 16 μF and 8 μF instead of the original 80 μF. The system ran easily with stability at only 8 μF of filter capacitance. Oscillation data for the thruster and array bus are shown in Fig. 12. (Capacitor oscillations are not shown; the current oscillations are very similar in magnitudes and trends to the thruster current and the voltage oscillations are very similar to the array voltage). There is no clear trend in thruster oscillations with capacitance; they are clearly independent of capacitance over this range. The thruster voltage oscillations have greater variations, and there may be a small systematic variation with capacitance but it is difficult to tell from these data. The array oscillations, however, can be seen to steadily increase as capacitance

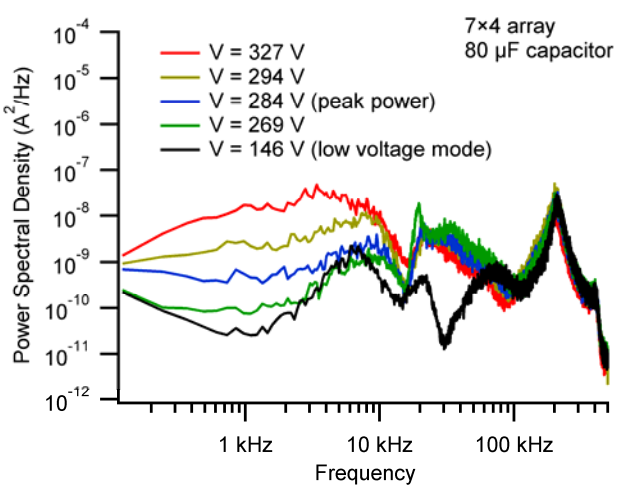

Fig. 11. Array Current Frequency Content.

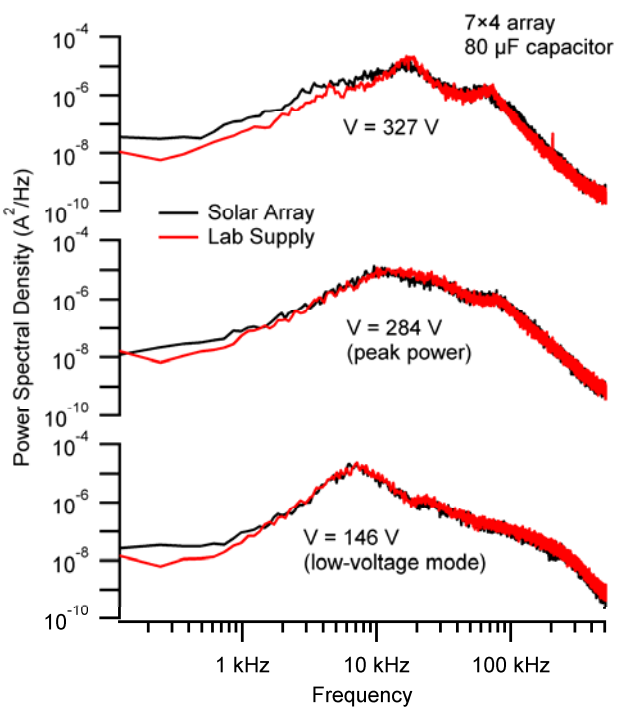

Fig. 10. Comparison of Thruster Current Frequency Content for Solar Array and Conventional Lab Supply.

is decreased, although they are still very small compared to the mean values of discharge current and voltage. It is also interesting to note that the voltage at which the thruster transitioned into the low-voltage mode did not show a significant dependence on the capacitor size. Although stable operation with smaller capacitances may be possible it is not clear that there are advantages to this (e.g. mass, cost), and larger capacitances could be desirable for other reasons (e.g. for startup transients).

A further investigation of the effects of filter capacitance was performed at identical thruster operating conditions. Data from this test, conducted with a 6×6 array operating at about 50% of the peak power, are shown in Fig. 13. There appears to be no change in thruster oscillation levels over this 16-57 μF range of filter capacitances and only a slight increase in the array oscillations, consistent with the results taken at different operating conditions. These results shown here suggest that a broad range of capacitance values are compatible with direct-drive Hall thruster operation, and that thruster operation is independent of the value of capacitance used. Capacitance has only a small effect on the array oscillations.

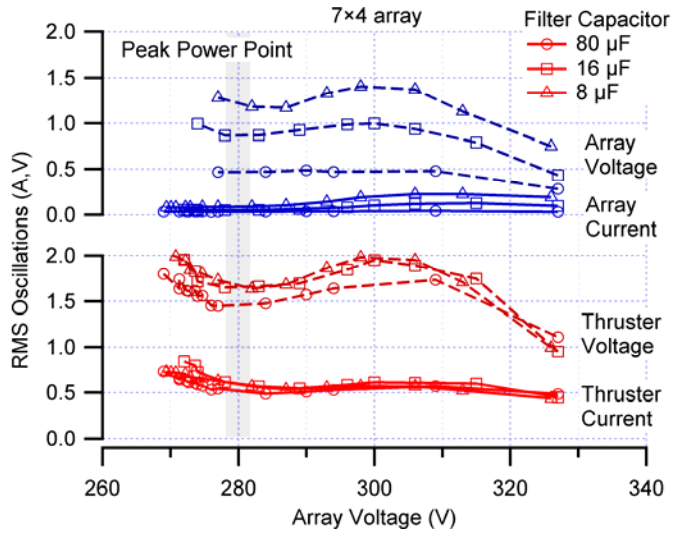

Fig. 12. Effect of Filter Capacitance on System Electrical Oscillations Measured Across the Current-Voltage Curve.

Operation at higher discharge voltages did not show any appreciable change in system RMS oscillations. Thruster and array current oscillations measured at voltages up to 430 V with a 9×4 array and 80 μF capacitor, shown in Fig. 14, were not significantly different from those measured at up to 330 V (Fig. 8), both of which had similar discharge currents. Limitations on voltage probes precluded collection of voltage data in this test. Again, magnet currents were not optimized in this test at each operating condition. Note that the thruster operated stably at voltages much less than the peak power voltage.

Operation at powers up to 10 kW, which represents an order-of-magnitude increase in power level over previously reported direct-drive tests, also did not show

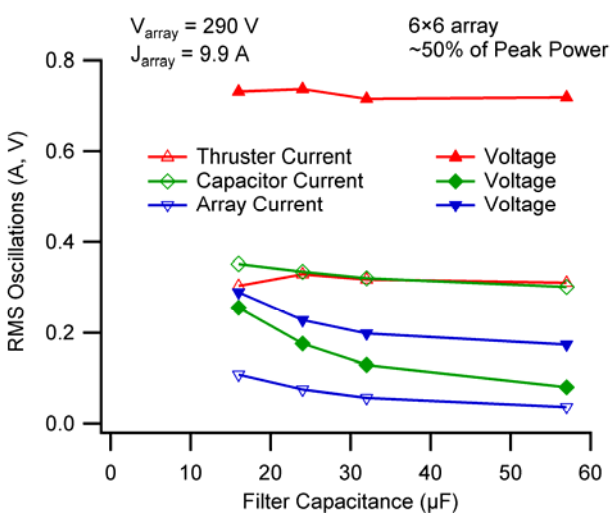

Fig. 13. Effect of Filter Capacitance on System Electrical Oscillations for a Single Operating Condition.

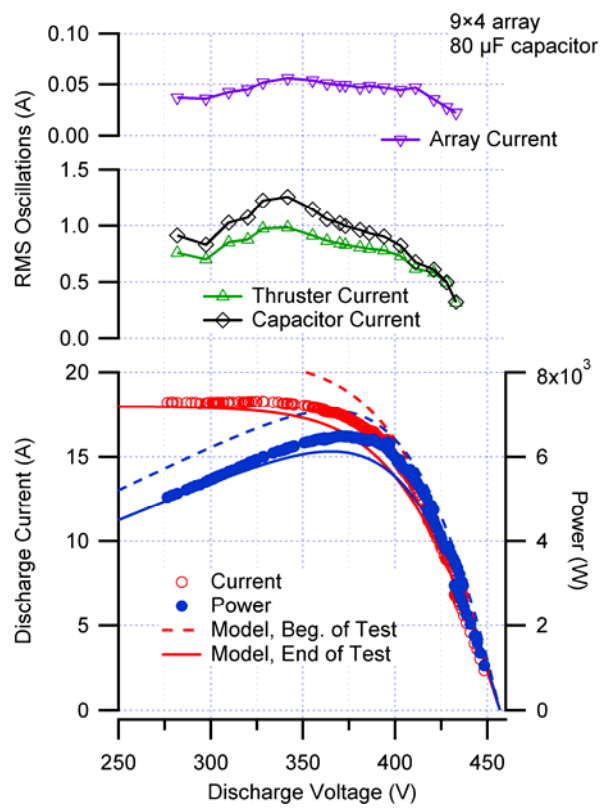

Fig. 14. System Operation at Higher Voltages.

any indication of anomalous behavior. Rather, current oscillations were relatively level and very small: less than about 5% of the mean current in the thruster and less than about 0.4% of the mean current in the array as seen in Fig. 15. The same was true of the system voltage oscillations. Thruster throttling over the P-V curve was no more difficult than for other array configurations with different voltages or powers.

The frequency spectra of the oscillations across the P-V curve at the higher voltages and higher powers were also examined. Although greater variations were seen than are present in Fig. 9 and Fig. 11, the similar general behaviors were observed.

It has already been shown that thruster current and voltage oscillations have little if any dependence on the size of the filter capacitor in the Direct-Drive system. A comparison of oscillation data acquired using the solar array and a conventional lab power supply at identical thruster operating points, shown in Fig. 16, demonstrates that thruster oscillations are the same independent of the power supply charging that filter capacitor. Although the filter capacitance was the same, the lab power supply had an output capacitance of 1000 µF making the total capacitance much different for the two systems. Thruster current oscillations are nearly identical for the solar array and lab supply operation, while there are some small differences in the voltage oscillations not unlike the differences seen in Fig. 12 for different capacitances. Analysis of the data collected in other test configurations suggests that this is not a systematic difference. Filter capacitor current and voltage fluctuations are of similar magnitudes for each power source, again with some minor differences. The largest difference observed is in the supply current oscillations, where surprisingly the solar array current oscillations were much smaller than for the lab supply, anywhere from 5 to 20 times smaller, even though the lab supply has large output capacitance. The general results discussed here pertaining to Fig. 16 held true for all direct comparison of operation on the solar array and on conventional supplies.

In summary, for direct-drive Hall thruster operation, thruster current and voltage oscillations are low compared to the mean values and show modest variations but no instabilities or anomalous operation across the array P-V curves, including operation at the peak power point. Further, thruster oscillations are independent of the value of filter capacitance (from 8 to 80 µF) and are the same as measured using conventional power supplies. Operation in the low-voltage mode does not cause dramatic changes in the oscillation frequency spectra. For the power system, current and voltage oscillations are very low compared to the mean values and exhibit

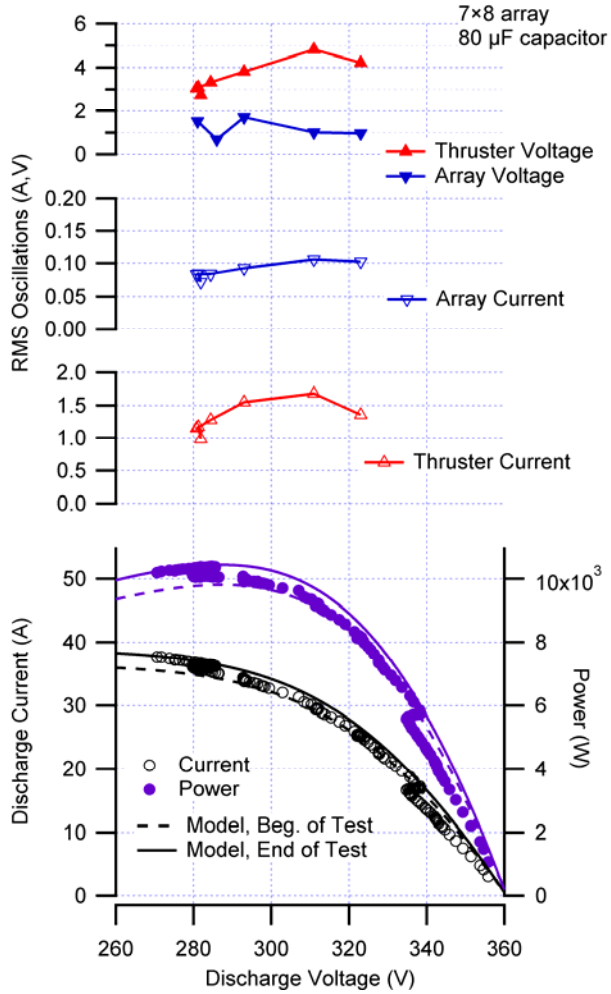

Fig. 15. System Operation at 10 kW.

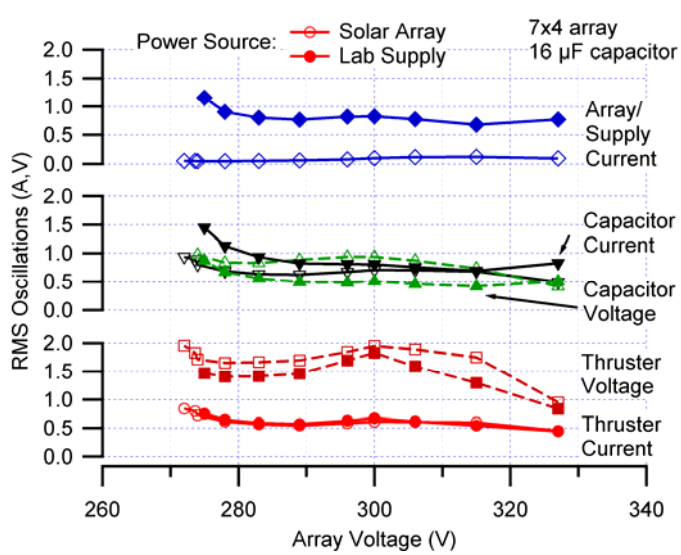

Fig. 16. Comparison of System Electrical Oscillations with Solar Array and Conventional Power Supply.

similar modest trends as the thruster oscillations across the array P-V curve. Slight systematic increases are observed as filter capacitance is decreased. No instabilities or anamalous behavior were observed in the power system at any operating condition from discharge voltages of 200-450V and discharge powers of 1 to 10 kW. There was no fundamental limit observed to direct-drive Hall thruster operation for any values of current, voltage, or power considered in this study.

C. Thruster Startup and Shutdown

Thruster startups with solar array power were first performed by rapidly applying voltage to the thruster anode after establishing steady cathode keeper current, anode flow, and magnet currents. Voltage was applied with an SCR switch installed in the power circuit between the filter capacitor and the thruster (as shown in the electrical schematic of Fig. 2). Measurement of the system response to the impulsive voltage application is shown in Fig. 17, where the propellant flow rates were set for a starting condition of 5 A discharge current at 300 V. The large thruster current inrush of 300 A in 40 µs leads to a set of large current and voltage spikes in the system: +500/-400 V in the thruster voltage, ±240 V in the capacitor voltage, and +30/-50 A in the current coming from the solar array. Spikes like these were frequently but not always observed, and did not appear to be controllable through changes in thruster flow rate or magnet setpoints. These large spikes were clearly undesirable, so an alternative startup method was investigated.

A softstart using the anode propellant flow as the system 'switch' was developed. Cathode keeper current and thruster magnet currents were first established, followed by application of the array open-circuit voltage to the thruster (at zero current). Next, anode flow was initiated. Because there were several meters of tubing between the mass flow controller and the engine, the discharge chamber pressure slowly increased from vacuum to a steady-state condition. Typically between twenty and forty seconds after initiating the anode flow, depending on the flowrate set point, the thruster ignited. Thruster current increased and voltage decreased until the discharge chamber pressure reached the steady state point.

Oscilloscope data from a typical softstart using an 80 µF capacitor are shown in Fig. 18. The thruster inrush current is about 80 A, much smaller than for the hardstart, and the power system current and voltage spikes have disappeared The thruster voltage spike is still present albeit at reduced levels; in the startup investigations performed here it was rarely larger than that shown in the figure. About 2 mC of charge was depleted from the 80 µF capacitor during this thruster current inrush which is small compared to the 29 mC of charge stored in the capacitor at the 370-V open-circuit voltage of the array. Hence, the voltage does not fall much and the array current slowly increases to replace the lost charge and sustain the steady-state thruster discharge current.

The effects of thruster flow rate, voltage, and magnet current on system response were investigated but none were shown to have a significant repeatable systematic effect. This type of softstart was used for most of the direct-drive testing and was shown to be a benign and reliable way to start the engine at all conditions including high voltages (Fig. 14) to initial powers as high as 4 kW (Fig. 6). Although higher-power softstarts have not yet been investigated there is no reason to believe there would be an issue.

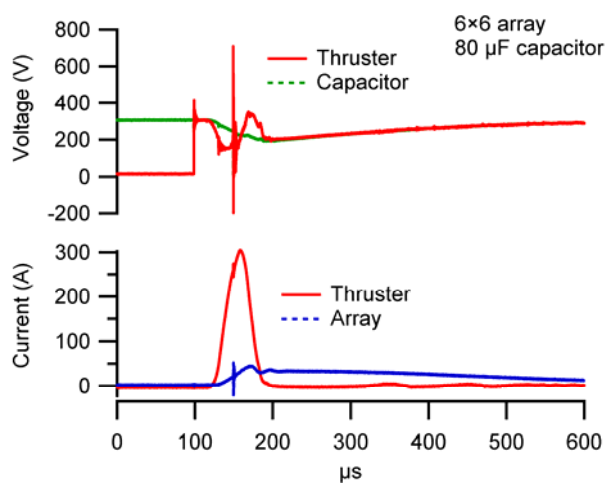

Fig. 17. System Response to Thruster Hardstart .

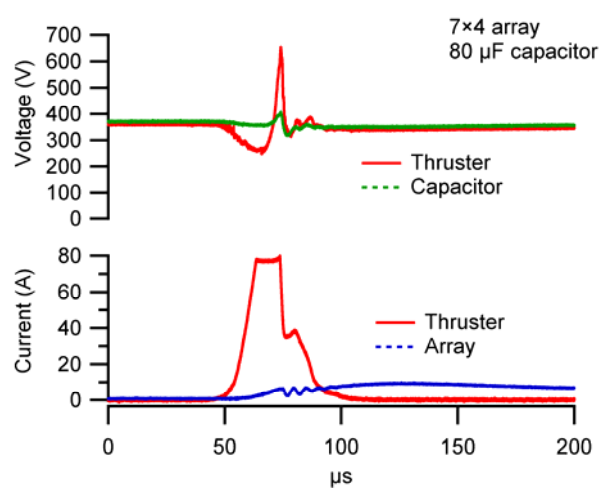

Fig. 18. System Response to Thruster Softstart.

An examination of system response to softstarts using different filter capacitances was performed in order to determine the capacitance necessary to source the thruster inrush transient. Shown in Fig. 19 are startup data acquired for three different filter capacitances, including the 80 µF data from Fig. 18. Note that the thruster current inrush is independent of the capacitor size for these tests. Higher array current and greater capacitor voltage sag transients are seen for the 16 µF capacitor compared to the 80 µF data. The stored charge in this capacitor is 6 mC, greater than the 2 mC of charge depleted by the thruster current inrush. Removal of that charge should drop the capacitor voltage to about 240 V, which is exactly what is seen in the data. The current from the array increases to replace that lost charge and rises to about 30 A, exceeding the ~20A short-circuit current of the array, meaning that stray capacitance in the array power system is providing charge to the capacitor and thruster on this timescale. Comparison with the array model shows that at about 75-100 µs after ignition the charge in this stray capacitance is exhausted and the array output falls back on the nominal I-V curve to recharge the capacitor and sustain the thruster discharge.

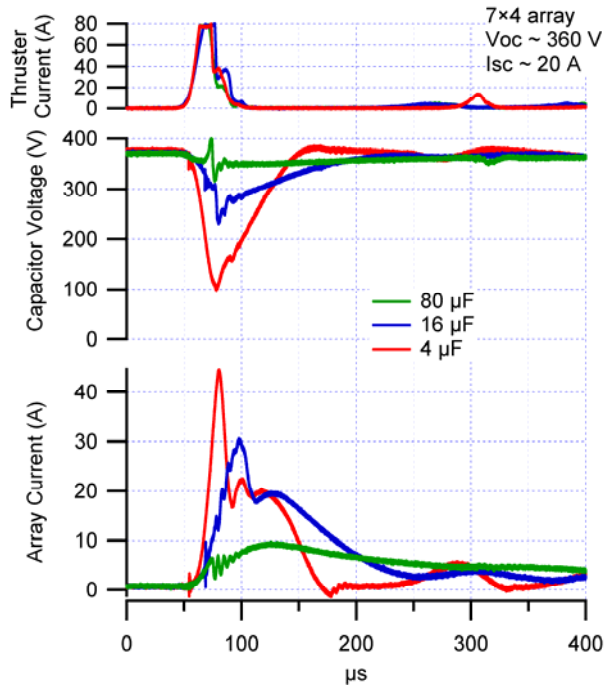

Fig. 19. Effect of Filter Capacitance on Power System Softstart Transients.

Greater voltage sag and higher current from the array system are seen for the startup with the 4 µF capacitor. Here the stored charge is 1.4 mC, less than the 2 mC thruster inrush. A greater inrush is seen from the power system stray capacitance, nearly 45 A, and the array returns to the nominal I-V curve at about the same time as for the 16 µF capacitor. The capacitor voltage sags to about 100 V during this event.

The stray capacitance in the array power system can be estimated by calculating the charge transfer from the system before the array falls back on the I-V curve. For both the 4-µF and 16-µF startups this charge transfer was 1.3 mC, indicating that the power system capacitance upstream of the filter capacitor is about 3.5 µF. This correlates well to the voltage sag seen in the 4-µF test. Here the total power system and filter capacitance is 7.5 µF. A loss of 2 mC of stored charge in this system due to thruster inrush would reduce the voltage to 100 V, exactly what is seen in the data.

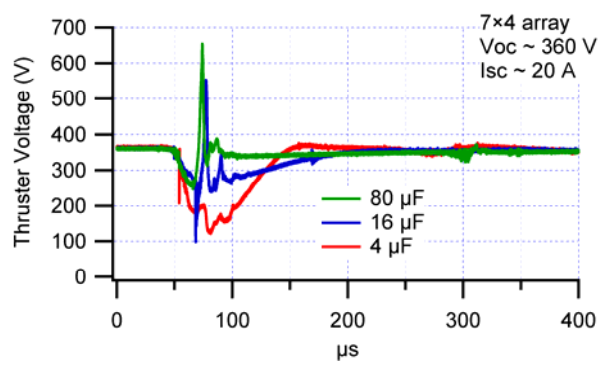

Fig. 20. Effect of Filter Capacitance on Thruster Voltage Softstart Transient.

Although power system transients increase in magnitude with decreasing filter capacitance size, the same is not true for the thruster voltage spikes observed at 80 µF as shown in Fig. 20. The large spikes are still seen at 16 µF, but at 4 µF the array/capacitor voltage sag has caused an accompany thruster voltage sag which has eliminated the voltage spikes. These competing effects suggest a balance in the total system capacitance may be warranted depending on system component requirements. For a flight implementation this would need further study.

Neither the power system nor the thruster appeared to suffer deleterious effects from the transients shown here and for the other cases investigated, and stable thruster operation was established in each case. Ultimately the solar array and thruster component requirements will have to be considered in direct-drive filter capacitor sizing, but here it is demonstrated that a wide range of sizes are acceptable and the power system response to softstarts is readily understood.

Thruster shutdowns by cutoff of propellant flow to the anode were also examined. One example is shown in Fig. 21 where cathode keeper current and thruster magnets were kept on at constant values during the shutoff. Discharge chamber pressure gradually decreased as the propellant in the length of tubing between the flow controller and the

thruster was depleted, and the thruster discharge extinguished after about three minutes. The thruster discharge was operating at 365 V and 0.2 A (80 W) just prior to extinguishing. System electrical oscillations were monitored over this time period and did not show any instabilities or anomalous behavior.

Demonstration of thruster softstarts and shutdowns by using anode flow control shows promising benefits for Direct-Drive system architectures. Specifically, the development of a high-voltage, high-current switch that must survive for hundreds or thousands of cycles for the Direct-Drive power system is not required. The system can be easily turned on and off by using the thruster propellant flow control as a switch.

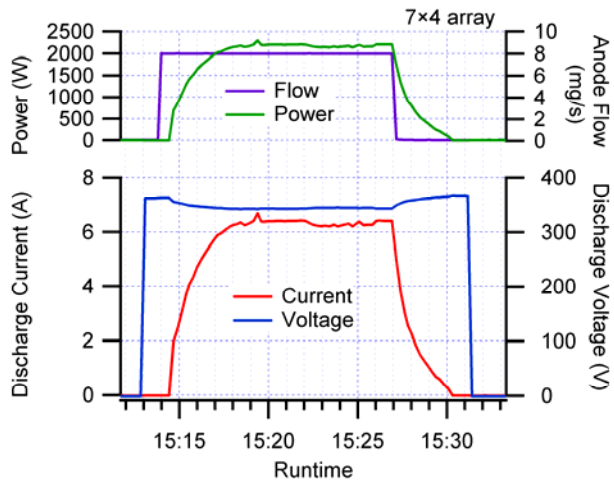

Fig. 21. Thruster Startup and Shutdown using Anode Propellant Flow Control.

D. Circuit Modeling

Modeling of the direct-drive electrical system with SPICE simulation software was initiated in order to develop a greater understanding of the system oscillation behavior and for use as a design tool. An example of a SPICE circuit developed for comparison with experimental data is shown in Fig. 22. The model incorporates only simple representations of circuit components and there are no adjustable parameters used for tuning to match calculations with experiment.

The solar array performance curve is defined by the current source I1, diode D1, and resistor R2, following the method of Rauschenbach.[29] Current I1 is the short-circuit current of the array at the time of the experiment. The series resistance R2, diode saturation current Is, and diode emission coefficient N are all calculated from the defining parameters of the I-V curve in the Rauschenbach model. This three-element SPICE model exactly reproduces the array I-V curves from the photovoltaic model used in this work and described in Section IIE. Because the array I-V curve changes with time in terrestrial application, in principle a different set of SPICE definition parameters is necessary for every experimental data point, although in practice one model can be applied to a short period of test data.

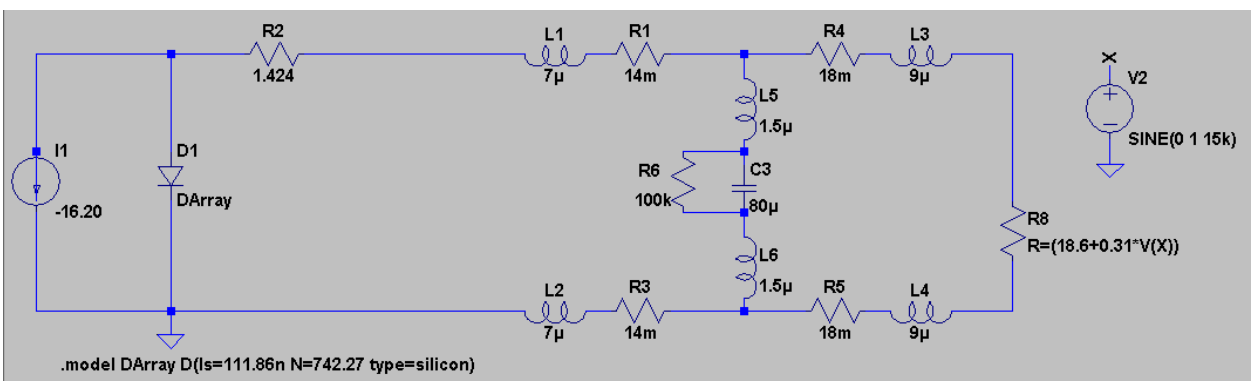

Fig. 22. SPICE Model of Direct-Drive System.

The thruster is modeled as a variable resistor R8, with the time-varying behavior incorporated using element V2. For this work a single frequency of 15 kHz was selected to model the approximate breathing mode frequency, although in principle modeling could be performed for any arbitrary frequency or, with more complicated models, a range of frequencies. The steady-state part of the resistance (18.6 ohms in Fig. 22) is selected to fix the point of thruster operation on the array I-V curve, while the time-dependent part of the resistance (0.31 ohms in Fig. 22) is selected to match the experimentally-measured discharge current oscillations. A simple sinusoidal variation in resistance and hence discharge current is assumed.

The filter capacitor is represented by C3 with the bleed resistor by R6. Also included are the calculated resistances of the wiring between the power control station and the capacitor (R1, R3) and between the capacitor and

the thruster (R4, R5). Calculated inductances of the wiring at 15 kHz are inserted to include this reactive component.

The SPICE model uses the measured thruster discharge current oscillations as the forcing function for the system oscillations. Array and capacitor current and voltage oscillations and thruster voltage oscillations can be easily calculated with the model and compared to experimental data. Experimentally it is observed that oscillations at many different frequencies can change depending on operating condition, therefore in this work only the RMS oscillations near the breathing mode were used for correlation. RMS oscillations between 10 and 20 kHz were calculated by integrating the power spectral density curves over this frequency range for each set of data, and those are the data presented here.

Correlation of experimental data to SPICE model results was examined for the data of Fig. 8 which were performed with a 7×4 array and an 80 µF filter capacitor. Four different sets of array definition parameters (I1, D1, R2) were used to span the seven experimental conditions. Shown in Fig. 23 are the measured thruster current oscillations near the breathing mode and the corresponding measured and calculated voltage oscillations. For this set of data the current and voltage oscillations have nearly the same magnitude but this is not a general result. The simple SPICE model captures the correct trends of the voltage oscillations but overpredicts them by about a factor of two.

Correlation with the array bus and capacitor current data, shown in Fig. 25, is much better. The SPICE model does a very good job of calculating the magnitudes of these oscillations although it does not quite capture the trend in array current oscillations at the highest voltages. The calculated voltage oscillations for the array and capacitor are nearly the same as seen in Fig. 24, although the measured data are further apart. Nonetheless, there is good agreement between the calculations and measurement for this simple SPICE representation of the direct-drive circuit.

SPICE model correlation was also performed for the single-operating-condition tests with different filter capacitances. Recall, these were performed with a 6×6 array at 290 V and 9.9 A, near 50% of the array peak power. Thruster RMS current oscillation measurements between 10-20 kHz, shown in Fig. 27, were used as the forcing function for the SPICE model. Thruster voltage oscillations near the breathing mode decrease as capacitance is decreased, in contrast to the near-constant oscillations seen over all frequencies in Fig. 13. Again the SPICE model overpredicts the thruster voltage oscillations but captures the correct trend.

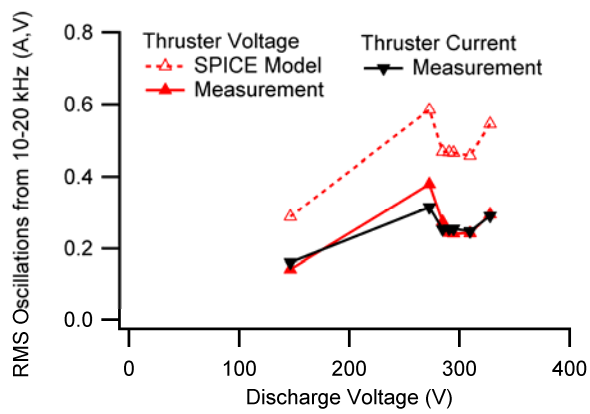

Fig. 23. Correlation of Thruster Voltage Oscillations with Model – Variable Voltage Case.

As for the earlier comparison at 80 µF, the SPICE model does a very good job calculating the array and capacitor current and voltage oscillations at 57 µF as seen in Fig. 26 and Fig. 28. As the filter capacitance is

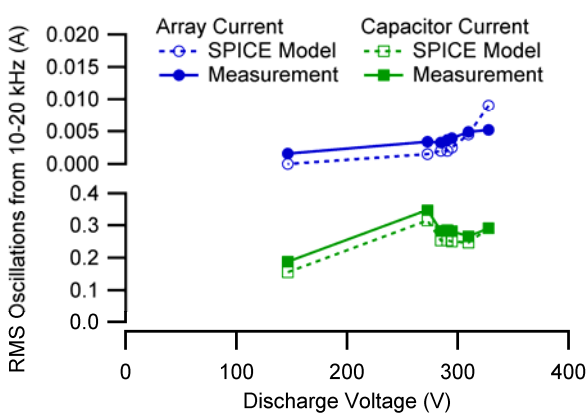

Fig. 25. Correlation of Power System Current Oscillations with Model – Variable Voltage Case.

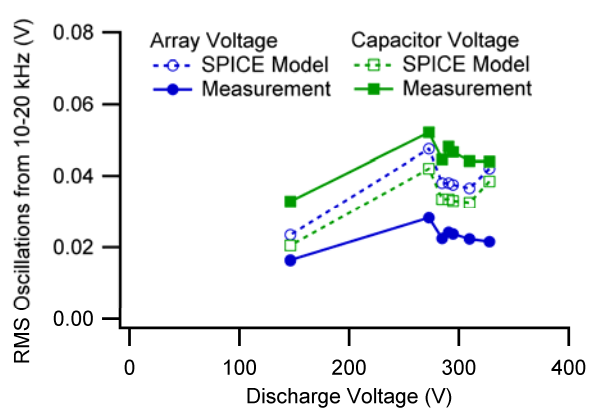

Fig. 24. Correlation of Power System Voltage Oscillations with Model – Variable Voltage Case.

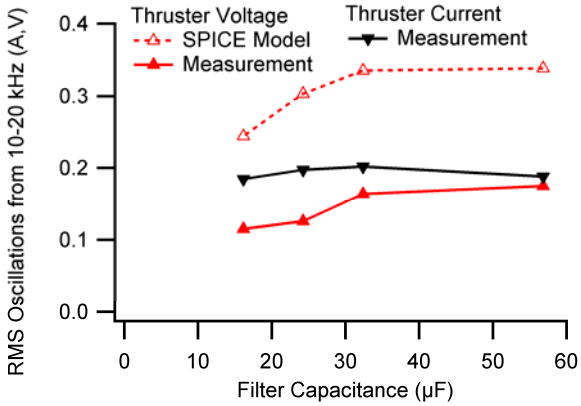

Fig. 27. Correlation of Thruster Voltage Oscillations with Model – Variable Capacitance Case.

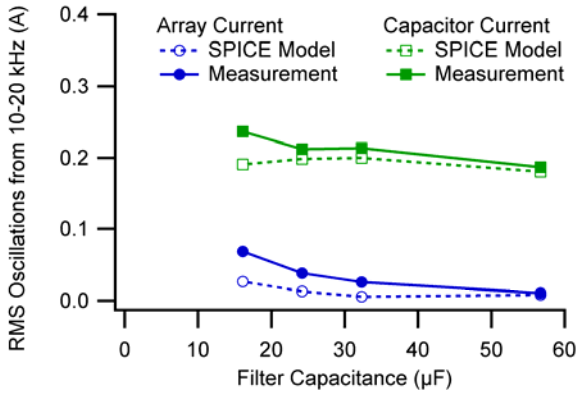

Fig. 26. Correlation of Power System Current Oscillations with Model – Variable Capacitance Case.

decreased the model captures the correct trends, but appears to produce progressively poorer results when compared to the measurements. This is likely due to increasing importance of stray reactance in the system that was not included, or perhaps in the case of the estimated wire inductances a difference between the calculation and the actual value. Nonetheless the magnitudes of the results are still good.

With this validation of the simple SPICE model, the model was next used to examine under controlled conditions the effects of variation in a single system parameter. Consider a system operating with a fixed solar array performance curve that produces a peak power of 6 kW at 300 V, the nominal full power operating point of the H6 thruster, with a short-circuit current of 21.4 A and open-circuit voltage of 370 V. System oscillations can be investigated for any filter capacitance at various points on the I-V curve while holding thruster current oscillations constant. The data of Fig. 12 and Fig. 13 showed that thruster current oscillations are independent of filter capacitance. While other data presented in this paper show modest variations in current oscillations as a function of location on the I-V curve (e.g. Fig. 8, Fig. 14, and Fig. 15), recall that the magnetic field was not optimized at each operating condition. Additionally, those variations are not large compared to the changes in mean discharge current level. Hence, the assumption of a constant thruster current oscillation can be meaningful in an investigation of system behavior.

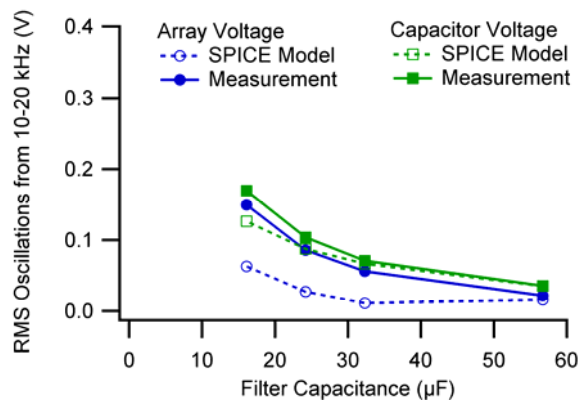

Fig. 28. Correlation of Power System Voltage Oscillations with Model – Variable Capacitance Case.

Shown in Fig. 29 is the dependence of array current oscillations on system capacitance at several voltages including the peak power voltage of 300 V. Array current oscillations are relatively flat until the filter capacitance is reduced to a value that depends on the location on the array I-V curve. On the flatter portion of the I-V curve (e.g. 200 V and 250 V) the array current oscillations are very small independent of capacitance. As the array I-V curve gets progressively steeper at higher voltages, array current oscillations get larger at the lower capacitances.

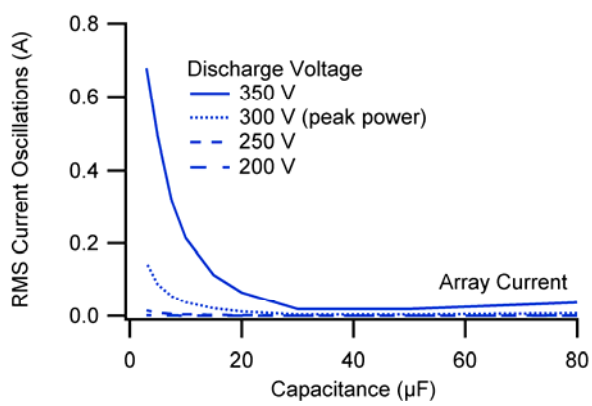

Fig. 29. Calculation of Effect of Filter Capacitance on Array Current Oscillations - Constant Thruster Current Oscillation Case.

Thruster and array voltage oscillations for these conditions are shown in Fig. 30. The array voltage oscillations are independent of voltage (i.e. location on the

I-V curve) and exhibit steep increases as capacitance is decreased below 20 µF. Thruster voltage oscillations are also largely independent of voltage, decreasing with capacitance until reaching a minimum near a few microFarads, then rising very quickly. These results at low capacitances should be considered qualitative since it has been shown that the SPICE model agreement with experimental data is poorer at lower capacitances. Recall, additionally, that startup transient testing indicated that capacitances less than 20 µF induced larger transients on the array bus. These results combined suggest that filter capacitances in the range of 20 to 60 µF are optimum for a direct-drive system like that one examined here.

A similar investigation was done to investigate the effects of different thruster current oscillations at a fixed capacitance of 30 µF. It was found that both the thruster and array voltage fluctuations are basically independent of voltage and have a linear dependence on thruster current oscillations over the range of 0.3 to 3.0 A_{rms}. Array current oscillations do vary with voltage as would be expected based on the position on the I-V curve, and also have a linear dependence on thruster current oscillations.

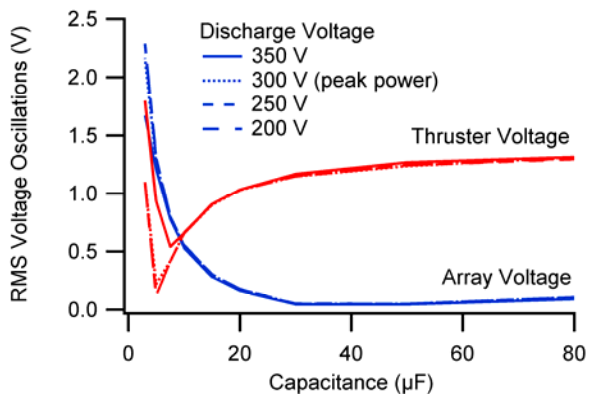

Fig. 30. Calculation of Effect of Filter Capacitance on Array and Thruster Voltage Oscillations - Constant Thruster Current Oscillation Case.

System oscillations were also investigated across the array I-V curve. Calculations using a fixed capacitance of 40 µF and fixed thruster RMS current oscillations of 0.7 A are shown in Fig. 31 along with the array performance curves. Smooth continuous behavior of the array oscillations and the thruster voltage oscillations is seen across the I-V curve, with nearly constant behavior at voltages less than the peak power voltage (the variations are nearly too small to see with a zero scale reference). It does not appear, for example, that thruster current fluctuations cause the operating point location on the I-V curve to experience wide swings in voltage near the flatter part of the I-V curve that could possibly drive the thruster into a low-voltage operating mode. Transition into the low-voltage operating mode does not appear to be an inherent property of the direct-drive system (as also evidenced by experimentally observed transitions into low-voltage mode when operating on current-limited conventional supplies).

In summary, there is nothing in the modeling results to suggest an inherent instability in the system when operating near and around the array peak power point, or at any other point on the I-V curve. Over the range of capacitances of interest in this study the same is true; although modeling has shown that oscillations can increase significantly at very low filter capacitance values, those low capacitances are not of practical interest because of the large startup transients observed on the power system.

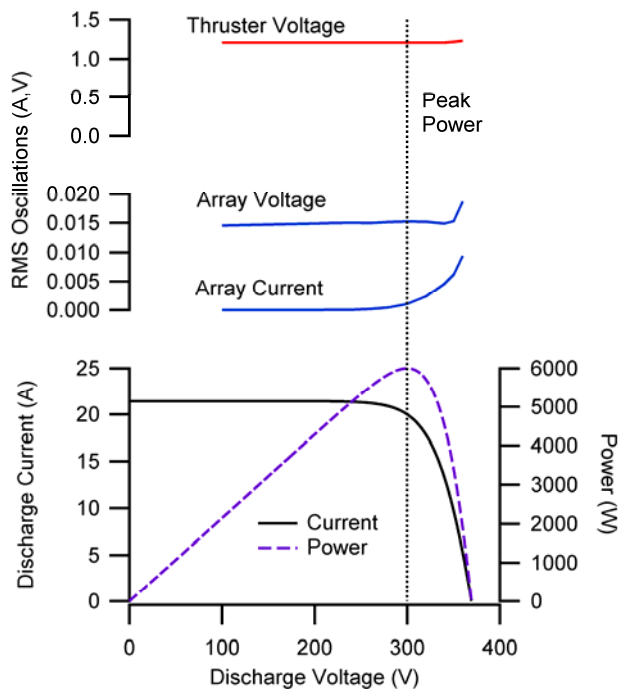

Fig. 31. Calculations of System Oscillations Across the Current-Voltage Curve – Constant Thruster Current Oscillation Case.

IV. Conclusion

A 12 kW solar array comprised of terrestrial commercially-available solar panels was designed and installed at the JPL Electric Propulsion Laboratory for investigation of direct-drive Hall thruster operation. A large series of experiments examining thruster control and operation, system electrical oscillations, filter capacitor sizing, and

thruster startup and shutdown methods were performed. For the first reported time, a Hall thruster was operated with a direct-drive power system at its full power design operating point. Operation of the H6 thruster was nominal with no instabilities or anomalous behavior observed over discharge voltages of 200 to 450 V and power levels of 1 to 10.4 kW. This is an order-of-magnitude increase in power over previously-reported direct-drive Hall thruster work. A photovoltaic performance model was developed and used to predict solar array performance curves and to correlate with thruster data to demonstrate system operation; the model was shown to closely match thruster test data.

The direct-drive Hall thruster system was easily controlled and operated in the same manner that a Hall thruster is controlled when using a conventional laboratory power supply or power processing unit (PPU). Thruster discharge current is controlled directly through the anode propellant flow rate; in the case of direct-drive operation this changes not only the discharge current but also the discharge voltage according to the solar array current-voltage curve. Thruster magnet currents are adjusted to tune the discharge current mean value and oscillations just as with a conventional power supply.

Direct-drive operation of a Hall thruster is the same as for operation with a conventional power supply. For the same discharge current and voltage settings the magnet currents and flow settings are the same. No special type of power system filtering is required, the same type of simple capacitor that is used in a conventional power system can be used.

Thruster operation and control is no different near and at the solar array peak power point than at any point with a greater voltage. In fact, from examining thruster data alone it is not possible to determine if the array is operating at the peak power or a greater voltage. Because the thruster can operate easily in a continuous fashion over this range, a solar array shunt regulator is not required.

In direct-drive operation the thruster will transition to a low-voltage operating mode at a voltage less than the peak power voltage that depends on the operating conditions. Experimental data shown here display this transition at anywhere from 20 to 100 V less than the peak power voltage. This transition to a low-voltage mode is not unique to a direct-drive system, it can be induced by operating with a conventional power supply while approaching the supply current limit. Recovery from a low-voltage mode into a normal operating mode was achieved in all instances simply by decreasing the anode propellant flow rate to reduce the discharge current and increase the discharge voltage.

The thruster can be started by rapidly applying voltage to it via a relay or thyristor, but it was found that this method led to large thruster inrush currents and power system transients. A more benign way to start the thruster is by using the anode propellant flow as the power 'switch'. With this method the array voltage can be switched to the thruster at zero current, obviating the need for high-current high-voltage relays. Reduced thruster inrush currents and power system transients were observed using this softstart method with low initial propellant flow rates. Thruster operation can quickly be ramped to full power after ignition. The thruster can also be shut off by stopping the anode flow rate to starve the discharge which was demonstrated to be benign to the power system.

Thruster and power system electrical oscillations were extensively investigated. Thruster oscillations measured during direct-drive operation were the same as for operation on conventional power supplies; current oscillations were nearly identical although there was greater variance in the voltage oscillations. These oscillations did not adversely affect operation of the solar array. With the wide range of filter capacitances investigated here the array oscillations were all extremely small compared to the mean values of current and voltage. Thruster and power system oscillations showed modest variation while transitioning from operation at voltages near the open-circuit voltage to the peak power point and to lesser voltages. Some of this variation may be because the thruster magnet currents were not optimized at every operating point. There was no indication of any instability or anomalous operation at any point on the solar array current-voltage curve investigated here. Oscillations in the low-voltage operating mode were not significantly noisier than in nominal operation and their frequency content was similar to nominal operation.

Experimental study of filter capacitance size showed that thruster operation and electrical oscillations are independent of capacitance over the range of 8 to 80 μF. Current and voltage oscillations in the solar array were observed to increase modestly as capacitance decreased in this range. Filter capacitances greater than 8 μF held sufficient charge to completely source the thruster inrush currents in the tests performed here, but even a capacitance of 16 μF led to appreciable solar array voltage sag during startup. An 80 μF capacitor minimized power system transients but led to larger thruster voltage transients. System studies including power system and thruster component requirements should be performed to determine the optimum filter capacitor size. The results of this study indicate that tens of microFarads of filter capacitance are sufficient to manage startup transients and steady-state electrical oscillations.

A simple SPICE model was developed and shown to capture enough of the direct-drive system physics to accurately model the trends and magnitudes of power system current and voltage oscillations. The model uses measured thruster current oscillations as a forcing function, and while it correctly captures the trends in thruster voltage it does a poorer job modeling the oscillation magnitudes. Calculations show that capacitances of a few to a few tens of microFarads are sufficient to dampen power system oscillations, depending on operating condition. SPICE model calculations also do not indicate any instabilities or anomalous system behavior across the solar array current-voltage curve.

In short, operation and control of the H6 Hall thruster using a direct-drive power system was shown to be simple and the same as with conventional power supplies. There were no fundamental limits on system operation observed in current, voltage, or power. System electrical oscillations were small compared to their mean values and no instabilities or anomalous behavior were observed.

Acknowledgments

The work described in this paper was carried out by the Jet Propulsion Laboratory, California Institute of Technology, under a contract with the National Aeronautics and Space Administration. Funding for this work was provided by the NASA Office of the Chief Technologist In-Space Propulsion Project. Special thanks to Ray Swindlehurst of JPL for his contributions to test setup and operation, and Hani Kamhawi of NASA Glenn Research Center for loan of the NASA-173M thrusters. A large number of people at JPL contributed to the design and installation of the solar array system, but we would specifically like to acknowledge the dedication and hard work of Tom Reed and Luba Berman. Mark Koehler, Ray Kariger, John Shuping, and Efren Escobedo also played instrumental roles. Thanks also to Cory Murphy of ELEN Consulting for photovoltaic electrical system design work.

References

1. Herron, B.G. and Opjordan, P.W., "High Voltage Solar Arrays with Integral Power Conditioning," AIAA Paper 70-1158, AIAA 8th Electric Propulsion Conference, Stanford, CA, Aug. 31- Sep. 2, 1970.
2. West, J.L., "Ion Drive Technology Readiness for the 1985 Halley Comet Rendezvous Mission," 78-641, AIAA/DGLR 13th International Electric Propulsion Conference, San Diego, CA, Apr 25-27, 1978.
3. Atkins, K., "Ion Drive: A Step Toward 'Star Trek'," AIAA 76-1069, Key Biscayne, FL, Nov 15-17, 1976.
4. Gooder, S.T., "Operational Compatibility of 30-centimeter-diameter Ion Thruster with Integrally Regulated Solar Array Power Source, NASA TN D-8428, July 1977.
5. Sauer, C.G., "Modeling of Thruster and Solar Array Characteristics in the JPL Low-Thrust Trajectory Analysis," 78-645, AIAA/DGLR 13th International Electric Propulsion Conference, San Diego, CA, Apr 25-27, 1978.
6. Stevens, N.J., et al., "Investigation of High Voltage Spacecraft System Interactions with Plasma Environments," 78-672, AIAA/DGLR 13th International Electric Propulsion Conference, San Diego, CA, Apr 25-27, 1978.
7. Parks, D.E. and Katz, I., "Spacecraft-Generated Plasma Interaction with High Voltage Solar Array," 78-673, AIAA/DGLR 13th International Electric Propulsion Conference, San Diego, CA, Apr 25-27, 1978.
8. Graf, J.E., et al., "Ion Propulsion Module Design and Mission Performance," 78-644, AIAA/DGLR 13th International Electric Propulsion Conference, San Diego, CA, Apr 25-27, 1978.
9. Hudson, W.R., "NASA Electric Propulsion Program," 78-711, AIAA/DGLR 13th International Electric Propulsion Conference, San Diego, CA, Apr 25-27, 1978.
10. Brophy, J.R., Barnett, J.W., Sankovic, J.M., and Barnhart, D.A., "Performance of the Stationary Plasma Thruster: SPT-100," AIAA-92-3155, IAA/SAE/ASME/ASEE 28th Joint Propulsion Conference and Exhibit, Nashville, TN, July 6-8, 1992.
11. Noca, M. and Brophy, J.R., "Over Powering Solar System Exploration," AIAA-97-2914, 33rd AIAA/ASME/SAE/ASEE Joint Propulsion Conference and Exhibit, Seattle, WA, July 6-9, 1997.
12. Hamley, J.A., "Hall Thruster Direct Drive Demonstration," AIAA-1997-2787, 33rd AIAA/ASME/SAE/ASEE Joint Propulsion Conference and Exhibit, Seattle, WA, July 6-9, 1997.
13. Jongeward, G.A., et al., "High Voltage Solar Arrays for a Direct Drive Hall Effect Propulsion System, IEPC-01-327, 27th International Electric Propulsion Conference, Pasadena, CA, Oct. 15-19, 2011.

14. Mikellides, I.G., et al., "Assessment of High-Voltage Solar Array Concepts for a Direct Drive Hall Effect Thruster System," AIAA-2003-4725, 39th AIAA/ASME/SAE/ASEE Joint Propulsion Conference and Exhibit, Huntsville, Alabama, July 20-23, 2003.
15. Schneider, T., et al., "Plasma Interactions with High Voltage Solar Arrays for a Direct Drive Hall Effect Thruster System," AIAA-2003-5017, 39th AIAA/ASME/SAE/ASEE Joint Propulsion Conference and Exhibit, Huntsville, Alabama, July 20-23, 2003.
16. Mikellides, I.G., et al., "Solar Arrays for Direct-Drive Electric Propulsion: Electron Collection at High Voltages," *J. of Spacecraft and Rockets*, Vol. 42, No. 3, May-June 2005, pp. 550-558.
17. Schneider. T. A, et al., "Solar Arrays for Direct-Drive Electric Propulsion: Arcing at High Voltages," *J. of Spacecraft and Rockets*, Vol. 42, No. 3, May-June 2005, pp. 543-549.
18. Hoskins, W.A., et al., "Direct Drive Hall Thruster System Study," JHU-CPIA: 51st JANNAF Propulsion Meeting, Orlando, FL, Nov. 2002.
19. Hoskins, W.A., et al., "Direct Drive Hall Thruster System Development, AIAA-2003-4726, 39th AIAA/ASME/SAE/ASEE Joint Propulsion Conference and Exhibit, Huntsville, Alabama, July 20-23, 2003.
20. Dankanich, J.W., "Direct Drive for Low Power Hall Thrusters," AIAA-2005-4118, 41st AIAA/ASEME/ SAE/ASEE Joint Propulsion Conference and Exhibit, Tucson, AZ, July 10-13, 2005.
21. Aintablian, H.O., Kirkhan, H., and Timmerman, P., "High Power, High Voltage Electric Power System for Electric Propulsion," AIAA-2006-4134, 4th International Energy Conversion Engineering Conference and Exhibit (IECEC), San Diego, CA, June 26-29, 2006.
22. Piszczor, M.F., et al., "The Stretched Lens Array SquareRigger (SLASR) for Space Power," AIAA-2006-4137, 4th International Energy Conversion Engineering Conference and Exhibit (IECEC), San Diego, CA, June 26-29, 2006.
23. Brandhorst, Jr., H.W., et al., "Direct-Drive Performance of a T-100 HET Powered by Triple Junction, High-Voltage Concentrator PV Array, AIAA-2010-6620, 46th AIAA/ASME/SAE/ASEE Joint Propulsion Conference and Exhibit, Nashville, TN, July 25-28, 2010.
24. Brophy, J.R., et al., "300-kW Solar Electric Propulsion System Configuration for Human Exploration of Near-Earth Asteroids," AIAA-2011-5514, 47th AIAA/ASME/SAE/ASEE Joint Propulsion Conference and Exhibit, San Diego, California, July 31-3, 2011.
25. Mercer, C., et al., "Benefits of Power and Propulsion Technology for a Piloted Electric Vehicle to an Asteroid," AIAA-2011-7252, AIAA SPACE 2011 Conference and Exposition, Long Beach, California, Sep. 27-29, 2011.
26. *CS5P-240/245/250/255/260M Datasheet*, Canadian Solar, Inc. Available from: www.canadiansolar.com/dl.php?dir=datasheets&file=CS5P-M_en.pdf [Cited May, 2012].
27. Haas, J. M., Hofer, R. R., Brown, D. L., Reid, B. M., and Gallimore, A. D., "Design of the H6 Hall Thruster for High Thrust/Power Investigation," Presented at the 54th JANNAF Propulsion Meeting, Denver, CO, May 14-17, 2007.
28. Snyder, J.S., T.M. Randolph, D.F. Landau, K.M. Bury, S.P. Malone, and T.A. Hickman, "Power and Propulsion System Design for Near-Earth Object Robotic Exploration," AIAA 2011-5662, 47th Joint Propulsion Conference, San Diego, CA, July 31 - Aug. 3, 2011.
29. Rauschenbach, H.S., *Solar Cell Array Design Handbook*. 1980, New York: Van Nostrand Reinhold. Section 2-33, Model 2.
30. Markvart, T., ed. *Solar Electricity*. Second ed., 2000, John Wiley & Sons, Ltd.: Chichester.
31. Duffie, J.A. and W.A. Beckman, *Solar Engineering of Thermal Processes*. Third ed., 2006, Hoboken: John Wiley & Sons, Inc.
32. Bird, R.E. and R.L. Hulstrom, *A Simplified Clear Sky Model for Direct and Diffuse Insolation on Horizontal Surfaces*, SERI report TR-642-761, Solar Energy Research Institute, Golden, CO, Feb. 1981.